



# A multi-control vehicle-to-grid charger with bi-directional active and reactive power capabilities for power grid support

Kang Miao Tan <sup>a, \*</sup>, Sanjeevikumar Padmanaban <sup>b</sup>, Jia Ying Yong <sup>a</sup>,  
Vigna K. Ramachandaramurthy <sup>a</sup>

<sup>a</sup> Institute of Power Engineering, Department of Electrical Power Engineering, Universiti Tenaga Nasional, Jalan IKRAM–UNITEN, 43000, Kajang, Selangor, Malaysia

<sup>b</sup> Department of Energy Technology, Aalborg University, 6700, Esbjerg, Denmark



## ARTICLE INFO

### Article history:

Received 19 October 2018

Received in revised form

7 January 2019

Accepted 13 January 2019

Available online 21 January 2019

### Keywords:

AC-DC power converters

DC-DC power converters

Electric vehicles

Power conversion

Reactive power control

Voltage control

## ABSTRACT

This paper proposes a multi-control vehicle-to-grid charger with bi-directional power capability. The proposed charger can perform vehicle battery charging and discharging operations, as well as power grid support such as reactive power compensation, power factor correction, and grid voltage regulation. The performances of the charger controls were examined under various power grid scenarios. Results revealed that the vehicle-to-grid charger attained the highest charger efficiency when operating at unity power factor mode. Nevertheless, vehicle charging at unity power factor introduced a significant grid voltage drop which may violate the grid voltage limits. This problem was solved by using the voltage control, which injected reactive power to the power grid for accurate voltage regulation. This paper also proposed an autonomous multi-control selection algorithm to intelligently switch between the multiple charger controls in response to the power grid condition. Results showed that the proposed algorithm effectively instructed the charger to work in efficient control modes if the grid voltage was within the permissible voltage limits. Whenever the grid voltage exceeded the limits, the charger automatically switched to grid voltage control for power grid voltage regulation.

© 2019 Elsevier Ltd. All rights reserved.

## 1. Introduction

In the twenty-first century, fossil fuel depletion and climate change have posed great challenges for the energy security. According to Ref. [1], electrifying the transportation sector is one of the main challenge in overcoming these issue. Over the past few years, the Electric Vehicle (EV) industry has shown a healthy growth. Major milestones of EV market were reported in the global EV outlook [2]. The global EV stock had reached 1.26 million units by the year 2015 [3]. It is also noteworthy to mention that the EV share in Norway had reached 23% and nearly 10% in the Netherland [2]. The global EV stock is projected to reach more than 100 million units on-road by the year 2050 with joint commitments between countries [4]. The number of EV charging stations have increased considerably since the electrification of the transport sector received public attentions. Up until July 2017, the registered public EV charging station had reached 100,000 units globally [5]. These

charging stations can provide the EV charging service, either in a slow, medium or fast mode.

The advancement of EV industry puts forward a state-of-the-art concept denoted as the Vehicle-to-Grid (V2G) technology. This technology can bring mutual benefits to both the power utility and EV owners. According to the research in Refs. [6,7], the integration of renewable energy into the electric grid can be greatly induced via V2G technology. From the perspective of power utility, the V2G technology utilizes the advanced charging facility to manage the vehicle storage energy for grid frequency regulation [8], demand response [9], energy reservation [10,11] and increase renewable energy generation [12]. Consequently, these grid support services can be realized without the need of additional investments on the storage system. Meanwhile, EV owners will be rewarded with incentives for providing services to the power grid [13].

The design of control strategy for the V2G technology is a popular topic in the recent literature. The active research and development in the EV technologies have stimulated the growth of EV industry. For instance, the authors in Ref. [14] designed a single-phase on-board EV charger. This charger can charge the EV battery

\* Corresponding author.

E-mail address: [tankangmiao@gmail.com](mailto:tankangmiao@gmail.com) (K.M. Tan).

and also provide reactive power compensation to the power grid based on the reactive power command from the utility. A fuzzy battery charger was proposed in Ref. [15] to charge the EV battery while operating at nearly unity power factor to reduce losses. This proposed charger utilized the ultra-sparse matrix rectifier to achieve the losses reduction. The authors in Ref. [16] introduced an EV fast charger with constant current/constant voltage charging operation. Similarly, the feature of power factor correction was considered in this fast charger. Another EV fast charger developed in Ref. [17] was capable of regulating the power grid voltage utilizing reactive power compensation. The proposed charger controller automatically detected the grid voltage drop during EV fast charging and injected an appropriate reactive power to regulate the grid voltage to a pre-set voltage level.

Apart from the uni-directional chargers, many bi-directional V2G chargers were proposed in the literature. The authors in Ref. [18] presented a bi-directional V2G charger which charged the EV battery during power grid off-peak period; whilst discharged the EV battery for grid support during on-peak period. The charger was designed to operate in a wide range of charging and discharging rates to achieve the load leveling and peak load shaving purposes. In Ref. [19], a Vehicle-to-Home (V2H) converter was proposed to utilize the EV battery as a power source in an islanded home electricity network. An active-reactive power control was adopted in the charger to provide a stable Home-to-Vehicle (H2V) charging and reactive power compensation for grid support. The authors further developed the V2H charger to provide the frequency and voltage regulation during the transition between grid-connected and islanded modes [20]. Another on-board V2G charger with bi-directional power flow capability was introduced in Ref. [21]. This charger provides dual directional active power exchange and power factor correction to the power grid. Similarly, a reduced capacity V2G charger developed in Ref. [22] was able to charge and discharge the EV battery while providing power factor correction to the grid.

In literature [23], the focus was on the bi-directional active power control design for V2G charger. The reactive power capability of the V2G charger was used to support the power grid [24,25]. These considerations lead to the design of reactive power control, power factor control, and grid voltage control. The variety of charger control options may complicate the planning process for the realization of the V2G technology. Hence, it is necessary to develop a V2G charger with a universal control strategy that can combine all the charger capabilities and react smartly to the power grid requirements.

In this paper, a multi-control V2G charger was proposed. The proposed charger had the bi-directional power capability to perform EV battery charging and discharging operations (active power control), as well as the reactive power compensation, power factor correction, and grid voltage regulation (reactive power control). Comprehensive analyses were executed to examine the performance of the charger controls under numerous power grid scenarios. From the results, the best practice for each charger control to meet specific application was recommended. Subsequently, a control selection algorithm was introduced to the multi-control V2G charger to automatically switch between the charger controls based on the power grid conditions. Overall, the main contributions of this paper are: (i) to design a multi-control V2G charger with the bi-directional active and reactive power capabilities to support the power grid, (ii) to develop a control selection algorithm for automatic switching between the multiple charger controls according to the power grid condition and requirement, and (iii) to perform comparative analyses and technical assessments on the proposed charger controls under various scenarios.

The rest of the paper is structured as follows: Section 2 details

the modeling of the V2G framework. The configuration and mathematical modeling of the proposed multi-control V2G charger are presented in Section 3. Section 4 discusses the technical comparisons and analyses for all the V2G charger controls. The control selection algorithm for multi-control V2G charger will be presented and analyzed in Section 5. Section 6 concludes the paper.

## 2. Power grid modeling for V2G integration

In this paper, a generic test network was modeled to examine the potentials of the proposed V2G charger and control. Several factors were considered in the designed power grid, which included the network practicality for V2G application, the sizing and placement of V2G chargers, as well as the availability and mobility of the grid-connected EVs. Since the power utility may require V2G services at any time whenever deemed necessary, the continuity to have available grid-connected EVs is essential to prevent any interruption during V2G operation. Thus, a township with both residential and commercial loads was designed to ensure high availability of grid-connected EVs and active EV mobility in the network.

Fig. 1 depicts the single-line diagram of the generic test network, which was modeled as a radial-configured power grid. The 132 kV bus had a fault level of 15.83 kA and was stepped down to the distribution voltage level of 11 kV by two 30 MVA transformers. The voltage level of the 11 kV main bus was set to 11.3 kV using the tap changer of the transformers to cater for the voltage drop issue in long cables. The bus section of the 11 kV main bus was closed to increase the power grid reliability. The total peak load demand of this test network was 23 MVA, which was within the rated capacity of each transformer ( $2 \times 30$  MVA).

The 11 kV switching bus received power from the upstream network via two 6 km length of 630 mm<sup>2</sup> single-core armoured aluminium cables to supply the residential-commercial township. As shown in Fig. 1, this township consisted of 17 substations that supplied residential loads; 16 substations that powered commercial areas; and nine substations that energized areas with a mixture of residential and commercial loads. There were a total of 42 substations across six feeders. Each substation supplied the low voltage loads through an 11/0.4 kV step down transformer with the rated capacity of 1 MVA. It was assumed that the residential loading was 100 kVA with a lagging power factor of 0.9; the commercial loading was 220 kVA with a lagging power factor of 0.95; and the mix loading was 170 kVA with a lagging power factor of 0.92. The complete description of the substation quantity and cable length of each feeder is presented in Fig. 1.

The V2G charger can be stationed at any substation provided that the maximum demand including the EV loading is within the rated capacity of the substation transformer. In this paper, the V2G chargers were connected at two substations (Sub-1 and Sub-38) for the power system study. This decision was made considering the test network boundaries by selecting the nearest and furthest substations from the switching bus.

## 3. Design of the multi-control V2G charger

Fig. 2 depicts the configuration of the proposed multi-control V2G charger, which was designed to have the bi-directional active and reactive power capabilities. This charger consisted of a three-phase full-bridge AC/DC converter, a DC-link capacitor, and a bi-directional buck-boost DC/DC converter. The V2G charger was connected to the power grid via a passive filter at the front-end while interacting with the EV battery at the back-end. Two controls were developed for the V2G charger to achieve different purposes, which include active power control and reactive power

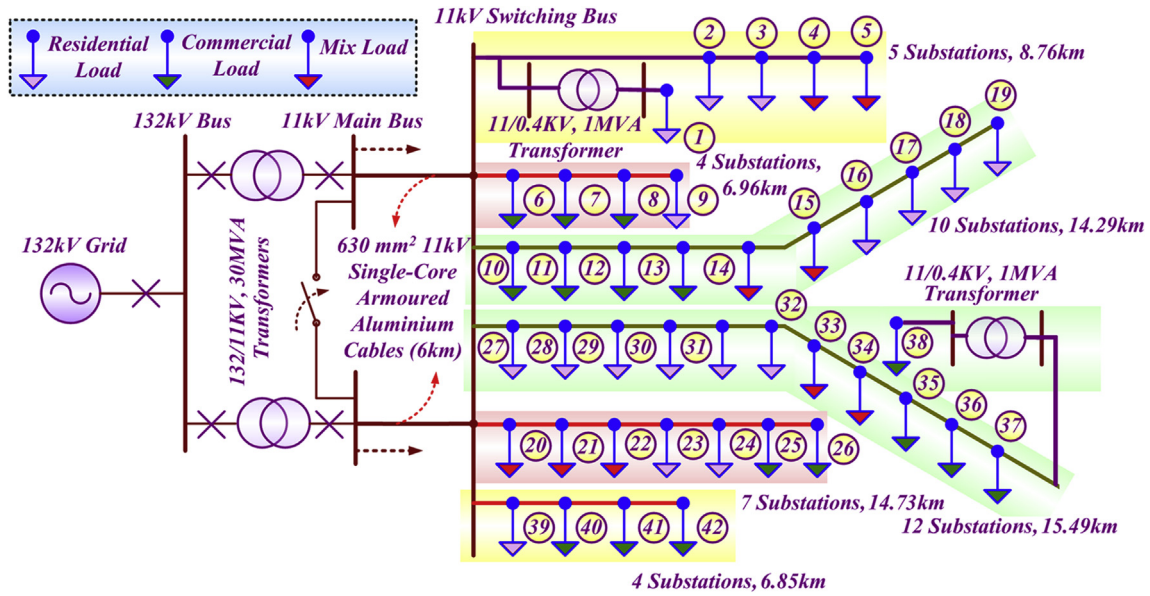


Fig. 1. Single-line diagram of the generic test network.

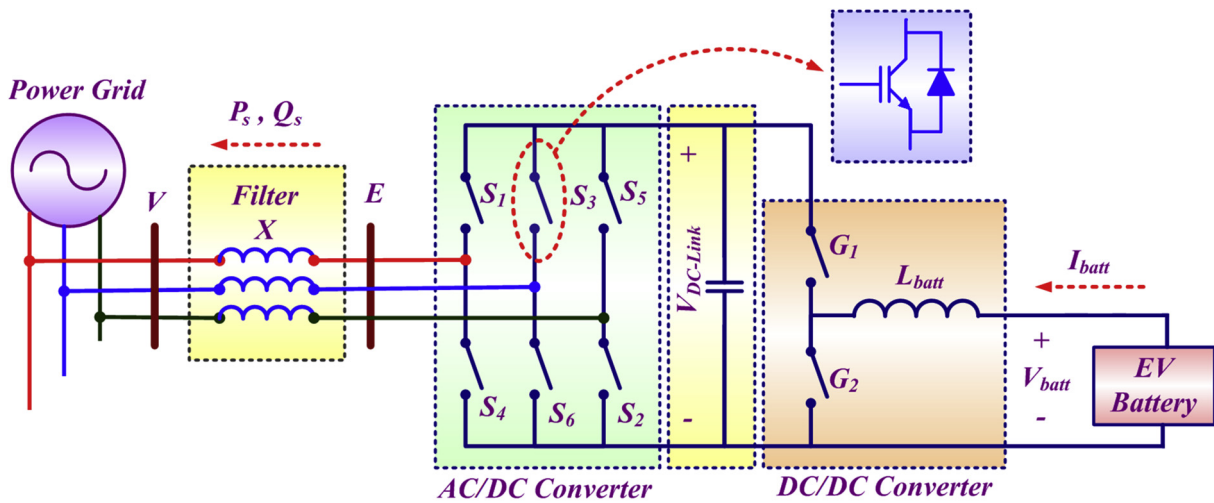


Fig. 2. Configuration of the proposed multi-control V2G charger.

control. The control strategies for active power control are as follows:

- Charging (C-control)

Active power flowed from the power grid into the V2G charger for EV battery charging. The charging power relied on the battery type and selected mode. In this research, slow charging consumed 3.3 kW, medium charging was rated up to 20 kW, and fast charging required 40 kW [26].

- Discharging (D-control)

EV battery discharged energy and supplied into the power grid through the V2G charger for active power support. The charger supported slow, medium, and fast discharging mode depending on the command from the power utility.

EV charging and discharging operations can affect the amount of energy stored in a battery. It is crucial to ensure the application of

an EV in the V2G technology does not affect the EV propulsion priority. Additionally, the EV battery State of Charge (SOC) and State of Health (SOH) shall also be considered carefully during its V2G application. Hence, battery SOC limits will be set during the V2G operation to prevent EV charging when the EV's SOC is more than the upper SOC limit; and to prevent the EV discharging when the EV's SOC is lesser than the lower SOC limit.

The V2G charger was also designed to supply reactive power for power grid support. The DC-link capacitor with appropriate control will act as a key element for the reactive power support. During the operation, the capacitor was charged and regulated to an appropriate voltage level which then acted as a source of reactive power to be injected into the power grid. Detailed mathematical explanation will be presented in Section 3.1. The control strategies for the reactive power control include:

- Direct reactive power (Q-control)

V2G charger absorbed/supplied reactive power from/to the

power grid based on a direct reactive power command from the power utility.

- Power factor (PF-control)

V2G charger controlled the reactive power flow to achieve a specific power factor. For this case, the input command to the charger controller was the power factor reference from the power utility.

- Grid voltage (V-control)

V2G charger injected or absorbed an accurate amount of reactive power to regulate the power grid voltage to a pre-set level, which was determined by the power utility.

Fig. 3 illustrates the four quadrant operations of the V2G charger. In this paper, the direction of power flow was defined to flow from the charger into the power grid, as shown in Fig. 2. Hence, the charger operations in Quadrant-I and Quadrant-IV were defined as EV battery discharging, while operations in Quadrant-II and Quadrant-III were defined as EV battery charging. On the other hand, the quadrant operations for Q-control depended on the direction of reactive power. When reactive power flowed from V2G charger into the power grid as presented in Quadrant-I and Quadrant-II, it was indicated as the capacitive operation. For Quadrant-III and Quadrant-IV, the V2G charger absorbed reactive power from the power grid. Thus, it was denoted as the inductive operation. Similar operations were applicable for V-control. When the grid voltage dropped below a pre-set voltage level, reactive power was injected into the power grid for grid voltage regulation, which was also defined as the capacitive operation. This operation dropped in Quadrant-I and Quadrant-II. Meanwhile, when the power grid voltage was more than a pre-set voltage level, V2G charger absorbed reactive power to reduce the grid voltage, which was similar to the inductive operation. This operation fell in Quadrant-III and Quadrant-IV. For PF-control, the power factor was defined as a lagging power factor whenever active power and reactive power were flowing in the same direction (Quadrant-I and Quadrant-III). In contrast, when active power flowed in the opposite direction from reactive power, it was indicated as a leading power factor (Quadrant-II and Quadrant-IV).

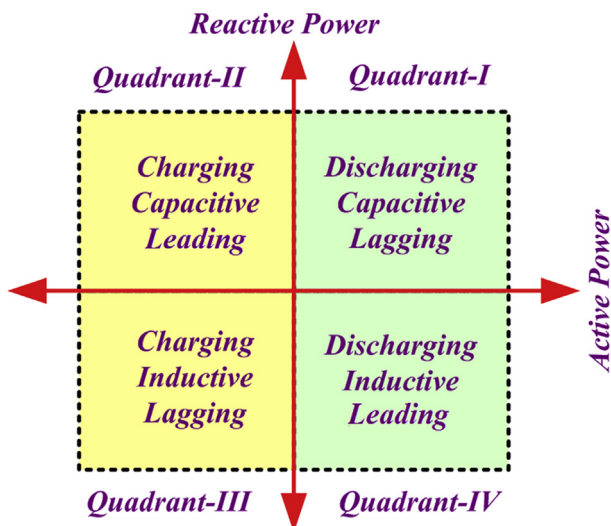


Fig. 3. Four quadrant operations of the V2G charger.

### 3.1. Mathematical analysis of the controller

This sub-section presents the mathematical analysis of the control strategies employed in the proposed multi-control V2G charger. The EV charging and discharging controls (C-control and D-control) were implemented in the bi-directional buck-boost DC/DC converter. Meanwhile, the three-phase full bridge AC/DC converter was in charge of conducting reactive power compensation, power factor correction, and grid voltage regulation using Q-control, PF-control, and V-control, respectively.

The DC/DC converter as shown in Fig. 2 allowed bi-directional power transfer between the power grid and EV battery. This converter operated as a buck converter during EV battery charging; whilst operated as a boost converter during EV battery discharging. Assuming a negligible converter loss, the governing equations for the DC/DC converter during charging operation is given as:

$$V_{batt} = D \cdot V_{DC-link} \tag{1}$$

$$P_{batt} = D \cdot V_{DC-link} \cdot I_{batt} \tag{2}$$

where  $V_{batt}$  is the battery voltage;  $D$  is the duty ratio;  $V_{DC-link}$  is the DC-link voltage;  $P_{batt}$  is the battery power, and  $I_{batt}$  is the battery current. Meanwhile, principle equations for the DC/DC converter during discharging operation is expressed as:

$$V_{batt} = (1 - D) \cdot V_{DC-link} \tag{3}$$

$$P_{batt} = (1 - D) \cdot V_{DC-link} \cdot I_{batt} \tag{4}$$

As presented in (2) and (4), the duty ratio ( $D$ ) of the DC/DC converter can be utilized to control the battery current ( $I_{batt}$ ), which in turn regulated the amount of battery power ( $P_{batt}$ ). A regulated DC-link voltage ( $V_{DC-link}$ ) can further smoothen the control of the DC/DC converter. Thus, the DC-link voltage ( $V_{DC-link}$ ) shall be one of the controlled parameters in the controller of the AC/DC converter.

On the other hand, the active power flow between the power grid and V2G system ( $P_s$ ) as shown in Fig. 2 can be represented by (5) [27]:

$$P_s = \frac{3 \cdot E_p \cdot V_p}{X} \sin \delta \tag{5}$$

$$\delta = \delta_E - \delta_V \tag{6}$$

where  $E_p$  is the phase voltage at the AC terminal of the AC/DC converter in root mean square;  $V_p$  is the power grid phase voltage in root mean square;  $X$  is the filter reactance;  $\delta$  is the phase shift angle between the grid voltage and charger converter's terminal voltage;  $\delta_E$  is the voltage angle of  $E_p$ , and  $\delta_V$  is the voltage angle of  $V_p$ .

In (5), the filter reactance ( $X$ ) had a fixed value; whilst the phase voltages ( $E_p$  and  $V_p$ ) and phase shift angle ( $\delta$ ) were variables. According to Ref. [27], the variation of phase shift angle ( $\delta$ ) had more significant effects on the active power flow ( $P_s$ ). Nevertheless, the active power flow across the V2G charger ( $P_s$ ) was solely used for EV battery charging and discharging, which was already managed by the controller of the DC/DC converter. As an alternative, the phase shift angle ( $\delta$ ) can be utilized to control the DC-link voltage ( $V_{DC-link}$ ) for several reasons: (i) to achieve a stable power matching between the AC/DC converter and DC/DC converter, (ii) to smoothen the charging and discharging controls of the DC/DC converter, and (iii) to provide reactive power capability for power factor correction, reactive power compensation, and grid voltage regulation. Therefore, the change in DC-link voltage ( $V_{DC-link}$ ) during EV charging and discharging operations will be compensated by varying the phase

shift angle ( $\delta$ ) using the proper control.

Another function of the AC/DC converter's controller was to employ the reactive power control using Q-control, PF-control, and V-control. For Q-control, the reactive power flow between power grid and V2G system ( $Q_s$ ) can be represented by (7) [27]:

$$Q_s = \frac{3 \cdot E_p}{X} [E_p - V_p \cos \delta] \quad (7)$$

The filter reactance ( $X$ ) had a constant value; whilst the phase shift angle ( $\delta$ ) had been used in the DC-link voltage ( $V_{DC-link}$ ) control. Therefore, the difference in phase voltages ( $E_p$  and  $V_p$ ) was utilized to control the amount of reactive power ( $Q_s$ ) [27].

The PF-control achieved power factor correction by adjusting the reactive power flow between the power grid and V2G charger ( $Q_s$ ). Using the power triangle concept, the relationship between reactive power flow ( $Q_s$ ) and power factor is described by (8):

$$Q_s = P_s \cdot \tan [\cos^{-1}(PF)] \quad (8)$$

where  $PF$  is the power factor. Considering (7) and (8), the power factor ( $PF$ ) can be rewritten as (9):

$$PF = \cos \left[ \tan^{-1} \left( \frac{3 \cdot E_p}{P_s \cdot X} (E_p - V_p \cos \delta) \right) \right] \quad (9)$$

The filter reactance ( $X$ ) had a fixed value and the phase shift angle ( $\delta$ ) was used in the DC-link voltage ( $V_{DC-link}$ ) control. The active power flow across the V2G charger ( $P_s$ ) was exclusively used for charging and discharging controls, which was managed by the controller of the DC/DC converter. Thus, the variation in phase voltages ( $E_p$  and  $V_p$ ) can be used to control the power factor ( $PF$ ) using the appropriate control.

The V-control was designed to utilize the reactive power capability of V2G charger to provide power grid voltage regulation. By rearranging (7), the grid phase voltage ( $V_p$ ) can be written as (10):

$$V_p = \frac{1}{\cos \delta} \left( E_p - \frac{Q_s \cdot X}{3 \cdot E_p} \right) \quad (10)$$

As presented before, the filter reactance ( $X$ ) and the phase shift angle ( $\delta$ ) served other purposes of the control. Therefore, the phase voltages ( $E_p$  and  $V_p$ ) difference was used here to achieve the power grid voltage regulation. In other words, the phase voltage at the AC terminal of the V2G charger ( $E_p$ ) can be utilized to control the grid phase voltage ( $V_p$ ) by injecting the appropriate amount of reactive power ( $Q_s$ ) into the power grid.

Generally, the AC/DC converter achieved all the reactive power controls, namely Q-control, PF-control, and V-control, via the change in phase voltages of  $E_p$  and  $V_p$ . When  $E_p > V_p$ , reactive power was injected to the power grid from the V2G charger; when  $E_p < V_p$ , reactive power was absorbed by the V2G charger from the power grid; and when  $E_p = V_p$ , no reactive power was exchanged between grid and charger.

In brief, the proposed multi-control V2G charger realized the active and reactive power control utilizing dedicated control strategies implemented in the charger's converters. In the DC/DC converter, the controller manipulated the duty ratio ( $D$ ) in order to control the battery current ( $I_{batt}$ ), which in turn controlled the active power flow across the charger ( $P_s$ ). Meanwhile, the controller of the AC/DC converter was in charge of using the phase shift angle ( $\delta$ ) to regulate the DC-link voltage ( $V_{DC-link}$ ), as well as to utilize the converter's terminal voltage ( $E_p$ ) for achieving reactive power compensation, power factor correction, and grid voltage regulation. Adequate tuning of the Proportional-Integral (PI) controller was crucial to realize the proposed controls in the V2G charger. The

equation of the PI controller is expressed as (11):

$$u(t) = K_p \cdot err(t) + K_i \int_0^t err(t) dt \quad (11)$$

where  $u$  is the controller output;  $t$  refers to time;  $K_p$  is the proportional gain;  $err$  is the error between the reference and input parameters, and  $K_i$  is the integral gain.

In order to represent a grid-connected EV in the power grid, a lithium-ion battery was modeled using the electric circuit-based model [28]. The battery was modeled as a controlled voltage source connected in series with an internal resistance. The controlled voltage source is characterized as in (12):

$$V_{batt} = E_0 - R_{batt} \cdot I_{batt} - K \frac{Q_{batt}}{I_{batt} t - 0.1 Q_{batt}} I_{batt}^* - K \frac{Q_{batt}}{Q_{batt} - I_{batt} t} I_{batt} t + A \exp(-B \cdot I_{batt} t) \quad (12)$$

where  $E_0$  is the battery constant voltage;  $R_{batt}$  is the battery internal resistance;  $K$  is the polarization constant;  $C_{batt}$  is battery capacity;  $I_{batt}^*$  is the filtered current;  $A$  is the exponential zone amplitude, and  $B$  is the exponential zone time constant inverse.

### 3.2. Mathematical analysis of the controller

The controller design for the V2G charger is deliberated in this sub-section. Fig. 4 illustrates the control block diagram of the proposed C-control and D-control for the DC/DC converter. This controller is designed to conduct both charging and discharging operations using C-control and D-control, respectively. Initially, the reference of battery current ( $I_{batt,ref}$ ) is measured and analyzed by a comparator to identify the control. The comparator sends a control signal to Selector-1 and Selector-2 to pick the appropriate pulses for the converter gates according to the chosen control. For C-control, the error between reference of battery current ( $I_{batt,ref}$ ) and measured battery current ( $I_{batt}$ ) is determined and channeled to a PI controller to generate an informative gain. Subsequently, a Pulse Width Modulator (PWM) converts the gain into a switching pulse for the top Insulated-Gate Bipolar Transistor (IGBT),  $G_1$  of the DC/DC converter; whilst turns OFF the bottom IGBT,  $G_2$ . Similar processes are applied for D-control but the final step is implemented in a contrary manner, where the generated PWM switching pulse is delivered to the bottom IGBT,  $G_2$  while turning OFF the top IGBT,  $G_1$ .

Fig. 5 presents the control block diagram of the proposed V-control, Q-control, and PF-control for the AC/DC converter. The AC/DC converter conducts reactive power control using three different strategies, which are V-control, Q-control, and PF-control. Firstly, a control selector evaluates the input command by the power utility and switches to the appropriate control accordingly. As the main input parameter to the controller, the grid voltage ( $V$ ) is measured and converts into rotating frame components of direct voltage ( $V_d$ ) and quadrature voltage ( $V_q$ ) using the Park's transformation. For V-control, the obtained direct voltage ( $V_d$ ) is compared with the pre-set voltage reference ( $V_{d,ref}$ ). The computed error is sent to a PI controller to generate the magnitude of the modulating signal ( $mag$ ). Meanwhile, Q-control utilizes the control processes of V-control by substituting the pre-set voltage reference ( $V_{d,ref}$ ) based on the reactive power information. The error between the reactive power flow ( $Q_s$ ) and pre-fixed reactive power reference ( $Q_{ref}$ ) is measured and feed to another PI controller. This PI controller computes the appropriate voltage reference required to achieve the desired reactive power. Similarly, PF-control further adopts the

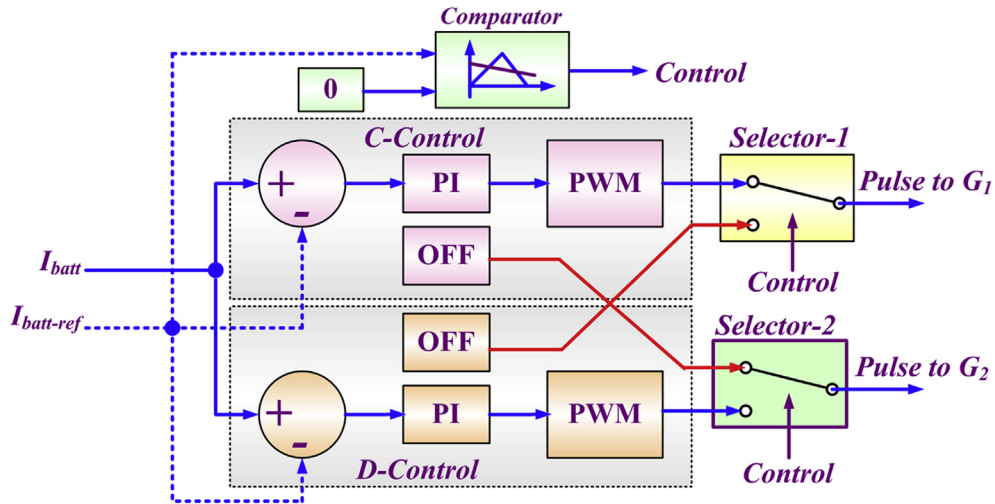


Fig. 4. Control block diagram of the C-control and D-control for DC/DC converter.

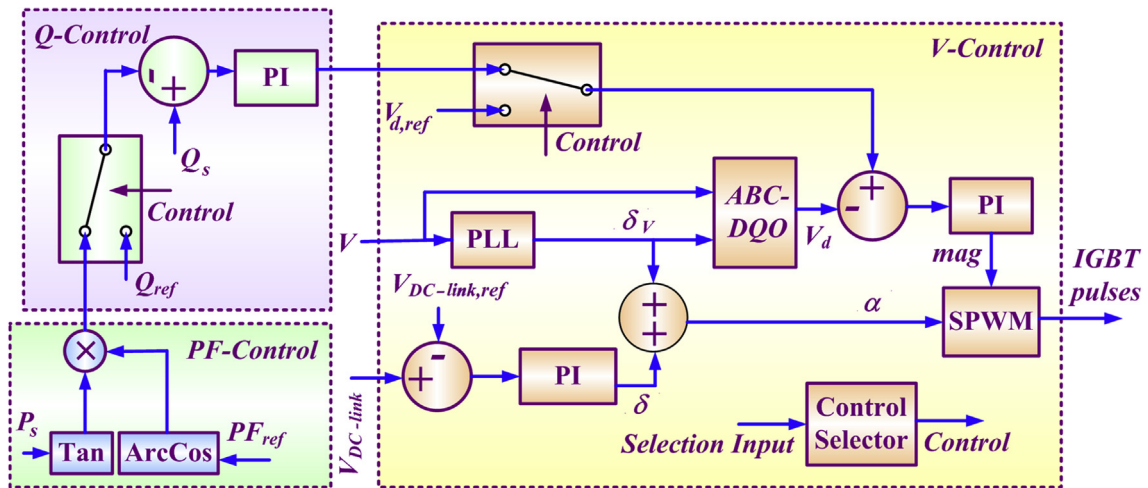


Fig. 5. Control block diagram of the V-control, Q-control and PF-control for AC/DC converter.

cascaded control concept by replacing the pre-fixed reactive power reference ( $Q_{ref}$ ) with the calculated reactive power based on the power factor information derived from (8).

As discussed in the previous sub-sections, the AC/DC converter is also in charge of regulating the DC-link voltage ( $V_{DC-link}$ ) to ensure stable operations of the V2G charger. For this control, the error between the DC-link voltage ( $V_{DC-link}$ ) and pre-fixed DC-link voltage reference ( $V_{DC-link,ref}$ ) is monitored. A PI controller responds to the detected error and generates a phase shift angle ( $\delta$ ) to regulate the DC-link voltage ( $V_{DC-link}$ ). For grid synchronization purposes, the measured grid voltage ( $V$ ) is channeled to a Phase-Locked Loop (PLL) to obtain the grid voltage angle ( $\delta_v$ ). The angle of the modulating signal ( $\alpha$ ) is obtained by adding the grid voltage angle ( $\delta_v$ ) with the phase shift angle ( $\delta$ ). As a result, a modulating signal with all the controlled information is acquired. The modulating signal is compared with a carrier triangular waveform to generate the switching pulses using the Sinusoidal Pulse Width Modulation (SPWM) technique. These pulses are sent to the IGBTs of the AC/DC converter to perform reactive power compensation, power grid voltage regulation, and power factor correction, as well as regulation of DC-link voltage ( $V_{DC-link}$ ).

#### 4. Comparative analysis and discussion

This section presents the simulation results to examine the performance of the active power control (C-control and D-control) and reactive power control (Q-control, PF-control and V-control) for the V2G charger using PSCAD/EMTDC software. The investigation was conducted in a V2G framework with multiple charger converters to demonstrate a practical V2G application. Fig. 6 shows the framework of V2G charging station used in this study, which allowed up to a maximum connection of 15 EVs. All V2G chargers are off-board charger, with the capability of providing fast charging to the EV. The proposed framework comprised of an AC/DC converter with 15 DC/DC converters connected via a common DC-link bus. In this paper, the rating of the V2G charger was sized to have sufficient capacity to support all the investigated scenarios. Generally, the setting of the DC-link voltage must be high enough for an excellent dynamic control but low enough to prevent unnecessary switching losses. The regulated DC-link voltage was determined to be 800 V while the DC-link capacitance was selected as 10,000  $\mu$ F. Table 1 presents all the parameter settings of the V2G charger.

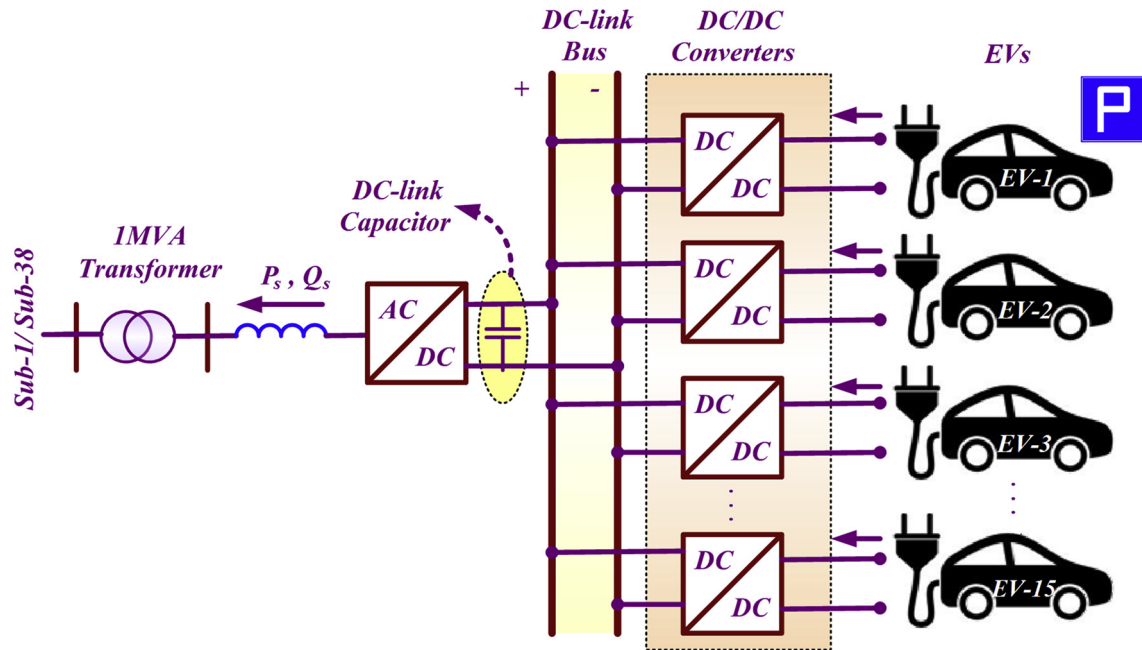


Fig. 6. Framework of V2G charging station.

**Table 1**  
Parameter setting of the V2G charger.

Parameter	Value
Grid voltage	400 V
Grid frequency	50 Hz
Filter inductance	0.1 mH
AC/DC converter's switching frequency	10 kHz
DC-link voltage	800 V
DC-link capacitance	10,000 $\mu$ F
DC/DC converter's switching frequency	10 kHz
Lithium-ion battery	360 V, 66.2 Ah

#### 4.1. V2G charging scenario

Various simulation scenarios were introduced to examine the voltage drop issue due to EV charging at Sub-38 as shown in Fig. 1, where the pre-charge voltage of this substation was 384 V or 0.96 p.u. of 400 V. Table S1 presents the controller setting and description for each charging scenario under different control modes. Every connected EV received fast charging current of 100 A. Meanwhile, the reactive power control was switched between Q-control, PF-control, and V-control modes. Each scenario underwent four different stages with an increasing number of grid-connected EVs. From  $t = 0$  s to  $t = 1$  s, no EV was connected; from  $t = 1$  s to  $t = 2$  s, five EVs were connected; from  $t = 2$  s to  $t = 3$  s, 10 EVs were connected; and from  $t = 3$  s to  $t = 4$  s, 15 EVs were connected.

EV charging along with Q-control was conducted under CQ1, CQ2, CQ3, and CQ4 modes. CQ1 and CQ2 modes worked in capacitive operation, whereas CQ3 and CQ4 modes worked in inductive operation. Fig. 7 depicts the comparative results of EV charging operation using Q-control. The results in Fig. 7(a) show a constant step decrease of active power in conjunction with the increased number of connected EVs for all control modes. Each connected EV received an approximately 40 kW of active power from the power grid. Fig. 7(b) shows that the V2G charger was capable of supplying and absorbing reactive power according to the pre-set reactive power reference. For CQ1 mode, reactive power was injected into the power grid, which prevented the expected grid voltage drop

due to the charging of EVs. As depicted in Fig. 7(c), the grid only experienced a slight voltage drop of 0.3 V for every connection of five EVs. For CQ2 mode, the charger injected twice amount of reactive power to the power grid compared to CQ1 mode. Instead of experiencing a voltage drop, the grid voltage had increased at an approximately 3 V for each EV charging stage. In contrast, V2G charger in CQ3 and CQ4 modes absorbed reactive power from the power grid and had led to a serious power grid voltage drop problem. Every successive connection of five EVs caused an approximately 7 V and 11 V of voltage drop for CQ3 and CQ4 modes, respectively. The grid voltage for both of these scenarios had dropped below 376 V, which violated the permissible voltage limit of  $-6\%$  [29]. Fig. 7(d) indicates that the proposed V2G charger was capable of regulating the DC-link voltage to 800 V, regardless of the connected EV numbers and control modes. From all the simulation results of EV charging with Q-control, it was noticeable that EV charging in capacitive mode was able to reduce the grid voltage drop issue due to charging of EVs itself, and even can improve the grid voltage. Meanwhile, EV charging in inductive mode led to a greater grid voltage drop problem. The voltage drop in CQ3 and CQ4 modes had caused poor dynamic response to the system, where significant fluctuations can be observed in the power and voltage waveforms, especially when 15 EVs were connected.

Fig. 8 shows the simulation results of EV charging operation using PF-control. This scenario consisted of three different modes of CPF1, CPF2, and CPF3, as described in Table S1. Fig. 8(a) indicates that each EV received an approximately 40 kW of charging power in all control modes. As shown in Fig. 8(b), in CPF1 mode, there was no reactive power exchange between the power grid and V2G charger as the charger was operated at unity power factor during charging of EVs. The grid voltage dropped by 3.9 V at every additional connection of five EVs in this mode, which is illustrated in Fig. 8(c). On the other hand, reactive power was supplied to the power grid from the V2G charger in CPF2 mode, which reduced the grid voltage drop impact. EV charging with a leading power factor of 0.9 only caused a minor grid voltage drop of 0.1 V for each EV connection. In CPF3 mode, both active and reactive power were drawn from the power grid into V2G charger. This situation led to a

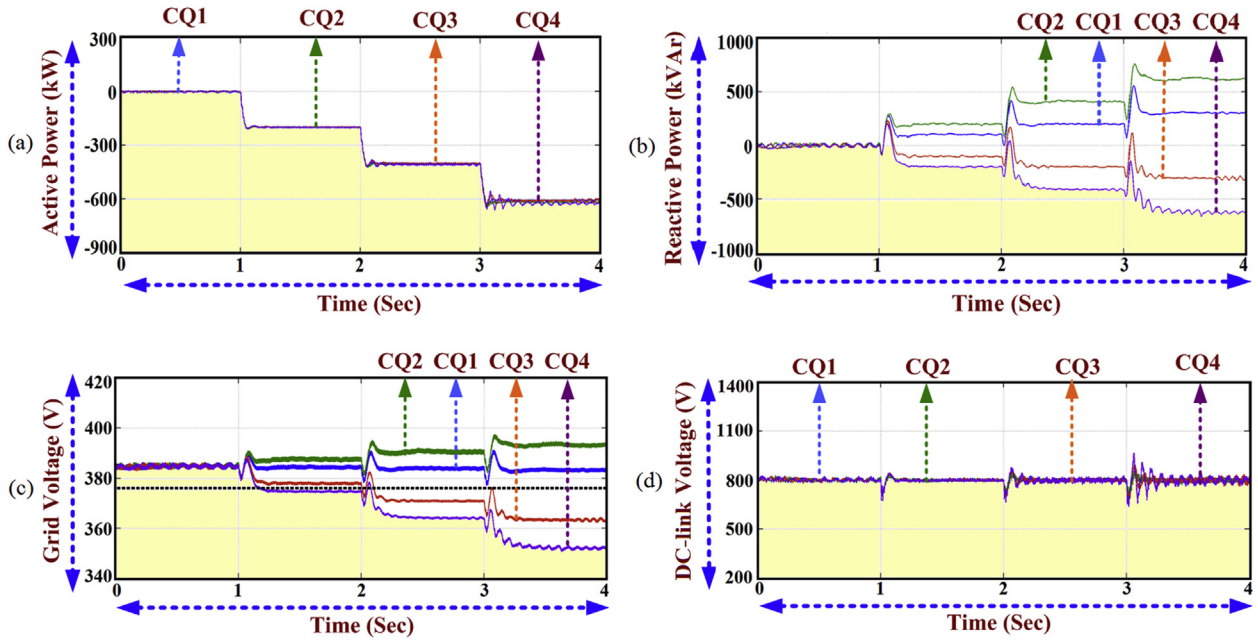


Fig. 7. Simulation results of EV charging with Q-control: (a) active power, (b) reactive power, (c) grid voltage and (d) DC-link voltage.

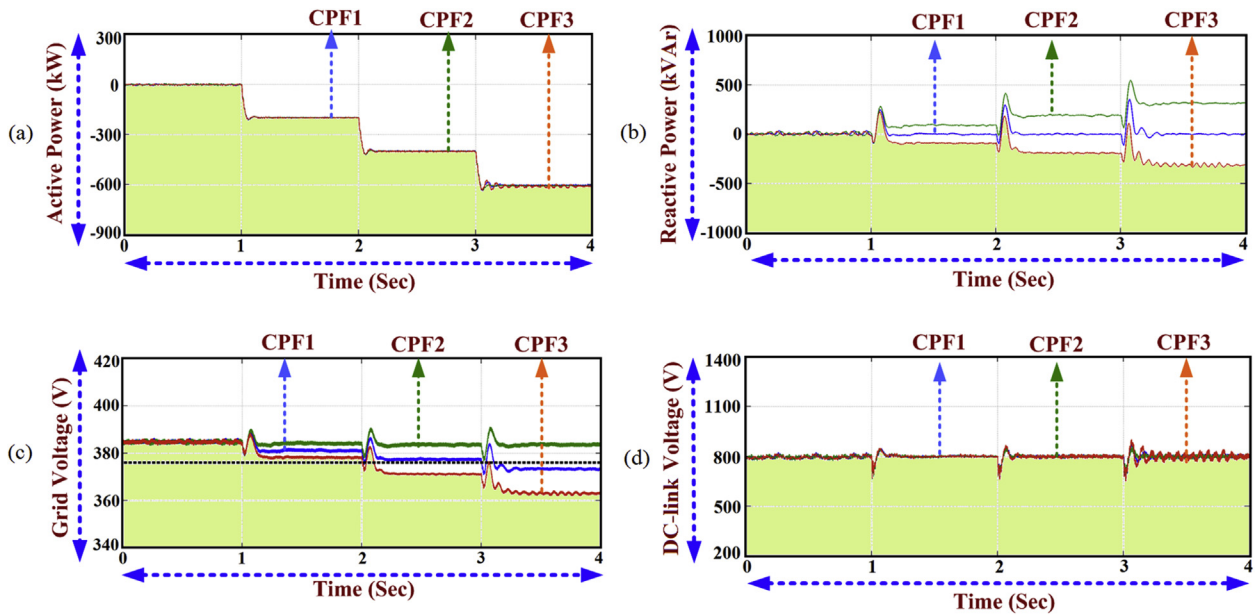


Fig. 8. Simulation results of EV charging with PF-control: (a) active power, (b) reactive power, (c) grid voltage and (d) DC-link voltage.

severe voltage drop at the power grid and eventually caused poor dynamic system response. As shown in Fig. 8(d), each PF-control mode was capable of maintaining the DC-link voltage at 800 V. The results in Fig. 8 present that EV charging at unity power factor still experienced noticeable grid voltage drop and even violated the minimum voltage limit of power grid when 15 EVs were connected. In the meantime, EV charging at a leading power factor can reduce the grid voltage drop issue; whilst EV charging at a lagging power factor led to a serious grid voltage drop problem.

EV charging operation using V-control was simulated in two control modes, which were the CV1 and CV2 modes. In CV1 mode, V2G charger charged EVs while regulating the power grid voltage to the pre-charge voltage of 0.96 p.u. Meanwhile, the power grid

voltage was regulated to 0.99 p.u. of 400 V during charging of EVs in CV2 mode. Fig. 9 presents the simulation results of EV charging with V-control. Similar to the other scenarios, V2G charger in both CV1 and CV2 modes was capable of supplying 40 kW of active power to charge each EV, as shown in Fig. 9(a). More reactive power was injected into the power grid from V2G charger when more EVs received charging. During EV charging processes, the controller of V2G charger provided an appropriate amount of reactive power to regulate the grid voltage based on the pre-set voltage reference, as presented in Fig. 9(b) and (c). The grid voltage was successfully regulated to pre-charge voltage of 0.96 p.u. in CV1 mode and to an improved voltage level of 0.99 p.u. in CV2 mode. Fig. 9(d) shows that the proposed V2G charger was capable of regulating the DC-

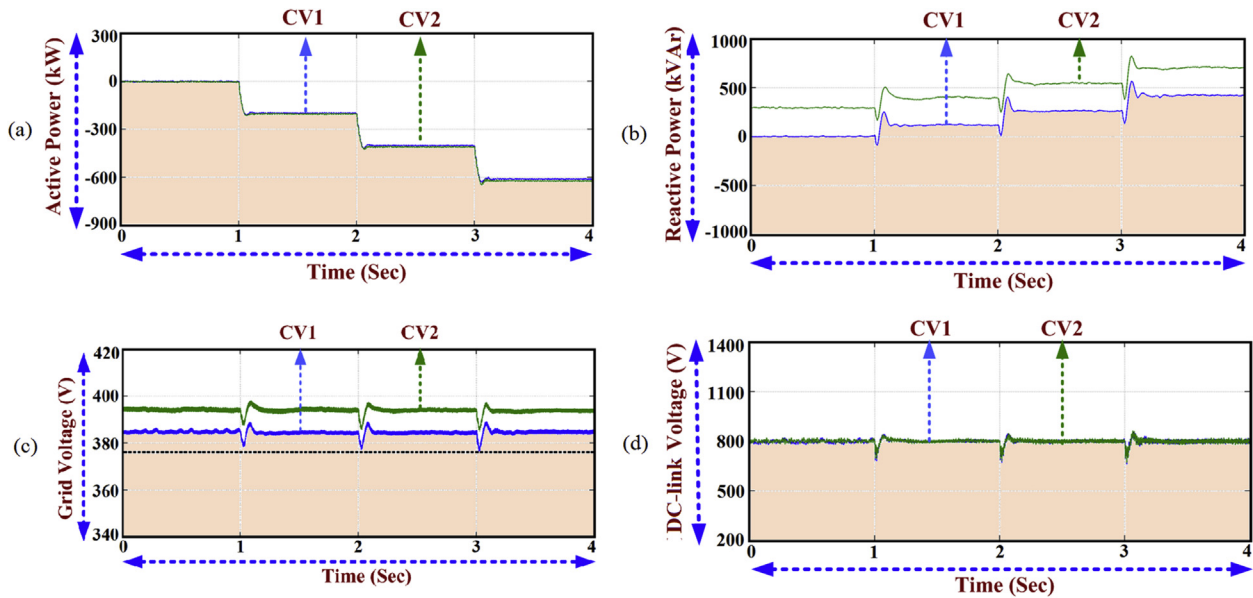


Fig. 9. Simulation results of EV charging with V-control: (a) active power, (b) reactive power, (c) grid voltage and (d) DC-link voltage.

link voltage to 800 V in all situations. In this V-control scenario, the controller had effectively regulated the grid voltage to pre-fixed voltage levels, which was achieved by the accurate management of reactive power flow. In CV2 mode, reactive power was injected to the power grid when there was no EV connection (from  $t = 0$  s to  $t = 1$  s) to regulate the grid voltage to a higher level. This situation showed that the control feature of grid voltage regulation can be implemented even when the grid-connected EVs were not presented.

In Fig. S1, the efficiency of V2G charger for each control mode was compared and analyzed. The charger efficiency was calculated using the active power from the power grid as the input power and the EV battery power as the output power. It can be observed that the charger efficiency was more than 90% in all the control modes. CPF1 mode (EV charging at unity power factor) marked the highest charger efficiency in every stage of charging operation.

Further investigation was conducted on the grid voltage throughout EV charging operation, as shown in Fig. S2. The studies in CQ3, CQ4, and CPF3 modes had experienced a serious voltage drop issue due to the absorption of reactive power during EV charging operation. Hence, these control modes would not be practical for implementation along with EV charging. CPF1 control mode had the highest efficiency but introduced a significant voltage drop to the power grid, which caused violation on the grid voltage limit during charging of 15 EVs. On the other hand, the studies in control modes of CQ1, CQ2, CPF2, CV1, and CV2 did not violate the minimum voltage limit of power grid in all operational stages. The reason was because the V2G charger was instructed to supply reactive power into the power grid, which reduced the voltage drop issue due to EV charging and even improved the grid voltage in some cases. Moreover, the comparative analysis in Fig. S2 indicated that CV1 and CV2 control modes had the least voltage fluctuation across each charging stage. This showed that V2G charger using V-control was capable of supplying reactive power to the power grid to accurately regulate the grid voltage to preferred levels.

#### 4.2. V2G discharging scenario

The investigation on the voltage rise issue during EV discharging

operation is presented in this sub-section. The proposed V2G charger was connected at Sub-1 as shown in Fig. 1, where the pre-charge voltage of this substation was 400 V. Table S2 presents the controller setting and description for each discharging scenario under different control modes. Each connected EV was instructed to discharge at 100 A while the reactive power control was switched between Q-control, PF-control, and V-control modes. Similar to the charging scenario in Section 4.1, each discharging scenario underwent four different stages with increased grid-connected EVs. From  $t = 0$  s to  $t = 1$  s, no EV was connected; from  $t = 1$  s to  $t = 2$  s, five EVs were connected; from  $t = 2$  s to  $t = 3$  s, 10 EVs were connected; and from  $t = 3$  s to  $t = 4$  s, 15 EVs were connected.

For Q-control, EV discharging operation was conducted under four control modes of DQ1, DQ2, DQ3, and DQ4. DQ1 and DQ2 modes operated in capacitive operation; while DQ3 and DQ4 modes worked in inductive operation. In Fig. 10(a), the active power increased for every stage of operation due to more EVs were discharging battery energy. Each EV discharged at 100 A and supplied an approximately 38 kW of active power to the power grid. Fig. 10(b) shows that reactive power was supplied and absorbed by the V2G charger according to the pre-set reactive power reference. For DQ1 and DQ2 modes, reactive power was injected to the power grid from the V2G charger, which had led to a significant grid voltage rise. For every connection of five EVs, the power grid experienced a voltage rise of around 4 V and 6 V for DQ1 and DQ2 modes, respectively. In contrast, charger operations in DQ3 and DQ4 modes absorbed reactive power from the power grid, which resulted in the grid voltage drop. Every successive connection of five EVs caused a voltage drop of an approximately 0.67 V for DQ3 mode and 2.67 V for DQ4 mode. As depicted in Fig. 10(d), the proposed V2G charger was capable of regulating the DC-link voltage to 800 V, regardless of the connected EV numbers and control modes. From all the simulation results of EV discharging along with Q-control, it can be observed that EV discharging in capacitive mode had led to an apparent increase in the grid voltage. On the other hand, the power grid experienced a slight voltage drop during the discharging event of EVs in the inductive mode. The operations of all four control modes in this scenario did not defy the power grid's permissible voltage limit of +10% and -6% [29].

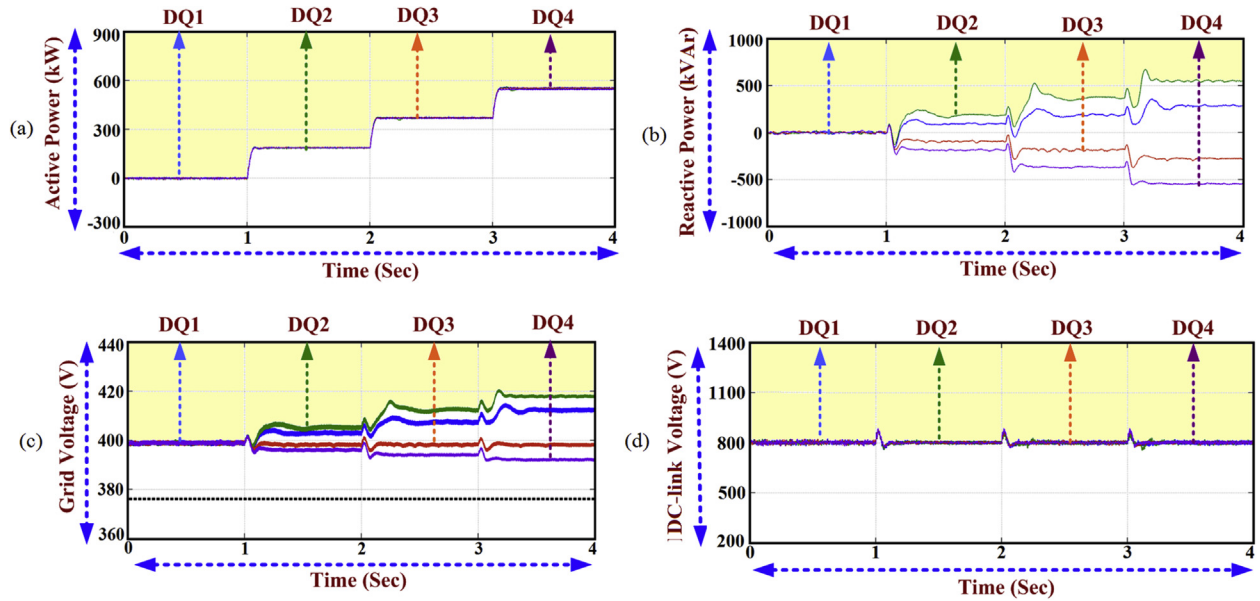


Fig. 10. Simulation results of EV discharging with Q-control: (a) active power, (b) reactive power, (c) grid voltage and (d) DC-link voltage.

Fig. 11 shows the simulation results of EV discharging using PF-control under DPF1, DPF2, and DPF3 modes. Fig. 11(a) shows that each EV contributed an approximately 38 kW of discharging power to the power grid in all control modes. Meanwhile, Fig. 11(b) shows that there was no reactive power exchanged between the power grid and V2G charger in DPF1 mode as the charger was operated at unity power factor. As illustrated in Fig. 11(c), every EV connection in this mode introduced a roughly 0.33 V of voltage rise to the power grid due to EV discharging power. On the other hand, the V2G charger absorbed reactive power from the power grid in DPF2 mode. Instead of causing voltage rise to the power grid, this control mode had resulted in slight grid voltage drop. During this control mode, each EV connection had caused a grid voltage drop of 0.12 V. In DPF3 mode, both active and reactive power were supplied to the power grid from the V2G charger. This had led to a notable voltage

rise at the power grid, where each additional EV had introduced approximately 0.83 V of voltage rise to the power grid. As shown in Fig. 11(d), each mode in PF-control was capable of maintaining the DC-link voltage at 800 V. The overall results presented that EV discharging at a lagging and unity power factor caused a significant voltage rise to the power grid. Nevertheless, EV discharging at a leading power factor reduced the voltage rise impact and can even cause voltage drop at the power grid.

Fig. 12 depicts the simulation results of EV discharging using V-control. This scenario consisted of two different modes, which were DV1 and DV2 modes. As shown in Fig. 12(a), each EV was capable of supplying 38 kW of active power to the power grid in both control modes. In Fig. 12(b), reactive power for both control modes showed a step decrease in every stage of operation. The reason was because the voltage rise due to each EV discharging was prevented utilizing

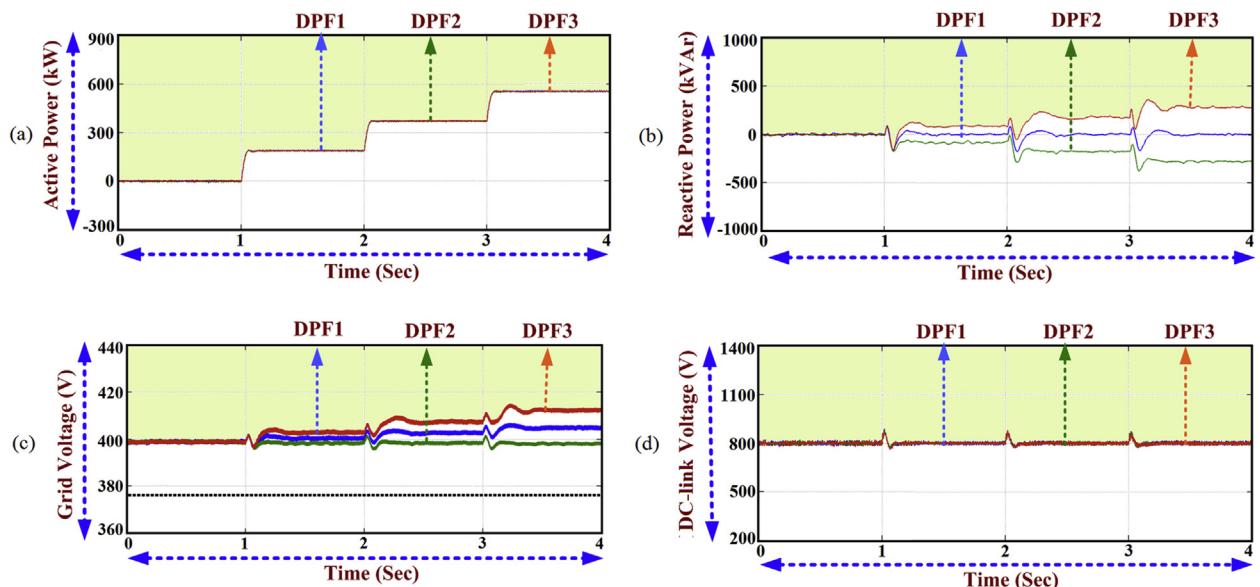


Fig. 11. Simulation results of EV discharging with PF-control: (a) active power, (b) reactive power, (c) grid voltage and (d) DC-link voltage.

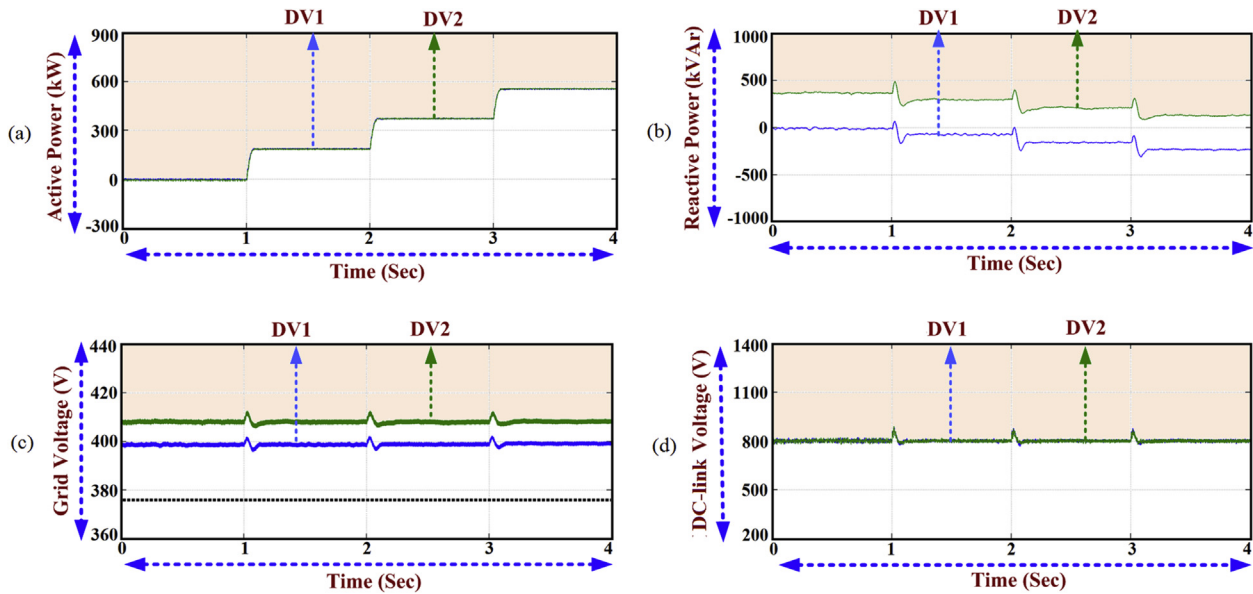


Fig. 12. Simulation results of EV discharging with V-control: (a) active power, (b) reactive power, (c) grid voltage and (d) DC-link voltage.

reactive power absorption by the V2G charger. Fig. 12(c) indicates that the control over reactive power flow had successfully regulated the power grid to pre-charge voltage of 1.00 p.u. in DV1 mode and to an improved grid voltage of 1.02 p.u. in DV2 mode. Meanwhile, Fig. 12(d) shows that the proposed V2G charger was capable of regulating the DC-link voltage to 800 V. In the V-control scenario, the charger controller showed an effective reactive power management to achieve an accurate grid voltage regulation. In DV2 mode, reactive power was injected to the power grid from  $t = 0$  s to  $t = 1$  s to improve the power grid voltage before any EV interconnection. This showed that the grid voltage regulation can be implemented using the V2G charger even when the grid-connected EVs were not available.

Fig. S3 presents the efficiency of V2G charger for each control mode during EV discharging. The charger efficiency was computed using EV battery power as the input power and the active power from the charger into the power grid as the output power. It can be noticed that all control modes had the efficiency larger than 90%. In average, DPF1 control mode (EV discharging at unity power factor) marked the highest charger efficiency.

Grid voltage analysis for all control modes during EV discharging operation was conducted, as shown in Fig. S4. Since EV discharging operation provided active power support to the power grid, voltage drop was not an issue for all discharging scenarios. Moreover, the voltage rise in DQ1, DQ2, DPF1, and DPF3 was not causing severe problem to the power grid. Hence, all V2G discharging scenarios were able to comply with the power grid voltage standard, which had the tolerable voltage limit of +10% and -6% [29]. Overall, EV discharging operation with V-control indicated the least voltage fluctuation across each evaluated stage. This showed that V2G charger using V-control had an excellent management and control over reactive power exchange delay ( $t_{delay}$ ), recorded reactive power ( $Q_{record}$ ), and reactive power margin for buffering purposes ( $Q_{buffer}$ ). The PF-control (unity power factor) was selected as the initial control mode for the V2G charger due to the highest power efficiency. The charger worked in PF-control as long as the grid voltage was within the pre-set voltage limits. Whenever these grid voltage conditions were not fulfilled, the charger control changed from PF-control to V-control in order to regulate the grid voltage to  $V_{max}$  or  $V_{min}$  for solving voltage rise or

voltage drop problem for accurate grid voltage regulation.

As presented in Section 4.1 and 4.2, the active power flow for all scenarios had negligible difference. This showed that the amount of reactive power flowed in and out of the charger had minimal impact to the active power. For benchmarking purposes, Table 2 shows the efficiency of the proposed charger compared to the other V2G chargers presented in the literature. The comparative analysis showed that the proposed charger in this paper achieved the highest efficiency percentile across all operation modes.

## 5. Multi-control selection algorithm

In the previous section, the results showed that the proposed V2G charger was capable of conducting EV charging (C-control) and EV discharging (D-control) while supporting the power grid with reactive power compensation (Q-control), power factor correction (PF-control) and grid voltage regulation (V-control). In all the control modes, the unity power factor using PF-control showed the best power efficiency in the V2G charger. However, voltage drop was an issue for this control operation during a larger scale of EV charging. Meanwhile, V-control was capable of automatically determining the accurate amount of reactive power required to achieve grid voltage regulation to desired voltage levels. V-control also showed a minimal voltage variance regardless of the numbers of grid-connected EVs. Hence, it can be summarized that the proposed V2G charger shall conduct EV charging and discharging utilizing PF-control to achieve unity power factor whenever the power grid voltage was within the permissible voltage limits. In the case of violation of grid voltage limits, V-control shall be adopted to regulate the power grid voltage to the permissible voltage limits of +10% and -6%. In this section, a multi-control selection

Table 2  
Comparison of V2G charger efficiency.

Control Mode	Highest Efficiency (%)			
	[14]	[15]	[21]	Proposed Charger
Q-control	92.00	N/A	N/A	97.98
PF-control	N/A	73.00	97.00	98.09
V-control	N/A	N/A	N/A	97.90

algorithm was proposed to assist the V2G charger in autonomous switching between PF-control and V-control according to the power grid voltage condition.

Fig. 13 presents the flowchart of the proposed multi-control selection algorithm. The initialization of the algorithm was performed by defining several parameters, such as the minimum grid voltage limit ( $V_{min}$ ), maximum grid voltage limit ( $V_{max}$ ), voltage margin for buffering purpose ( $V_{buffer}$ ), time correspondingly. Subsequently, a delay of  $t_{delay}$  was imposed to permit the control response settled to the steady state. The reactive power during steady state was recorded as  $Q_{record}$  and was compared with the measured reactive power ( $Q_s$ ). During this process, a reactive power margin ( $Q_{buffer}$ ) was introduced for buffering purpose to prevent inaccurate detection of the system response. Whenever the condition of  $Q_s > Q_{record} + Q_{buffer}$  or  $Q_s < Q_{record} - Q_{buffer}$  was met, it represented that the voltage rise or voltage drop issue had been improved. In other words, V-control was no longer required. Therefore, the charger control switched from V-control back to PF-control for higher charger efficiency. The recorded reactive power ( $Q_{record}$ ) was reset and the algorithm looped back for grid voltage monitoring.

Fig. 14 provides clearer insights on the interaction between the proposed V2G charger, Distribution System Operator (DSO), and power grid for a practical V2G application. The multi-control selection algorithm as well as the bi-directional active and reactive power control were all implemented in the proposed V2G charger. For a proper implementation, the DSO provided the control commands to the V2G system after assessing the power grid and EVs conditions. Based on the DSO's commands, the multi-control selection algorithm was executed to determine the appropriate

control to be implemented by the charger's AC/DC controller for power grid supports. V2G charger can provide reactive power compensation, power factor correction, and grid voltage regulation in response to the need of the power grid. Meanwhile, each DC/DC controller of the V2G charger received charging or discharging instruction directly from the DSO.

The effectiveness of the proposed multi-control selection algorithm in a practical V2G application as shown in Fig. 14 was investigated. The result findings in Section 4 showed that voltage drop was the main issue for the V2G implementation in this paper. Hence, EV charging scenario at Sub-38 was the only case study considered in this section. Fig. 15 depicts the simulation results of the implementation of multi-control selection algorithm in V2G charger. In Stage-I, EV was not connected to the V2G charger. There was no active and reactive power exchanged between the power grid and V2G charger. The grid voltage was 384 V while the DC-link voltage was maintained at 800 V. In Stage-II, six EVs were connected to the power grid via V2G charger for fast charging purposes. During this period, an approximately 240 kW of active power was drawn from the power grid to the charger. As shown previously in Fig. 13, the charger control was initially set to unity PF-control (control setting = 0). As a result, reactive power exchange between the power grid and charger was recorded to be 0 kVar. In this stage, the grid voltage had dropped to 380 V while the DC-link voltage was maintained at 800 V. In the following stage, the number of EV received fast charging increased to nine causing 360 kW of active power to flow from the power grid to V2G charger. The grid voltage in Stage-III dropped to 378 V and was still stayed within the pre-fixed voltage limits. Hence, the charger control remained operated in unity PF-control (control setting = 0).

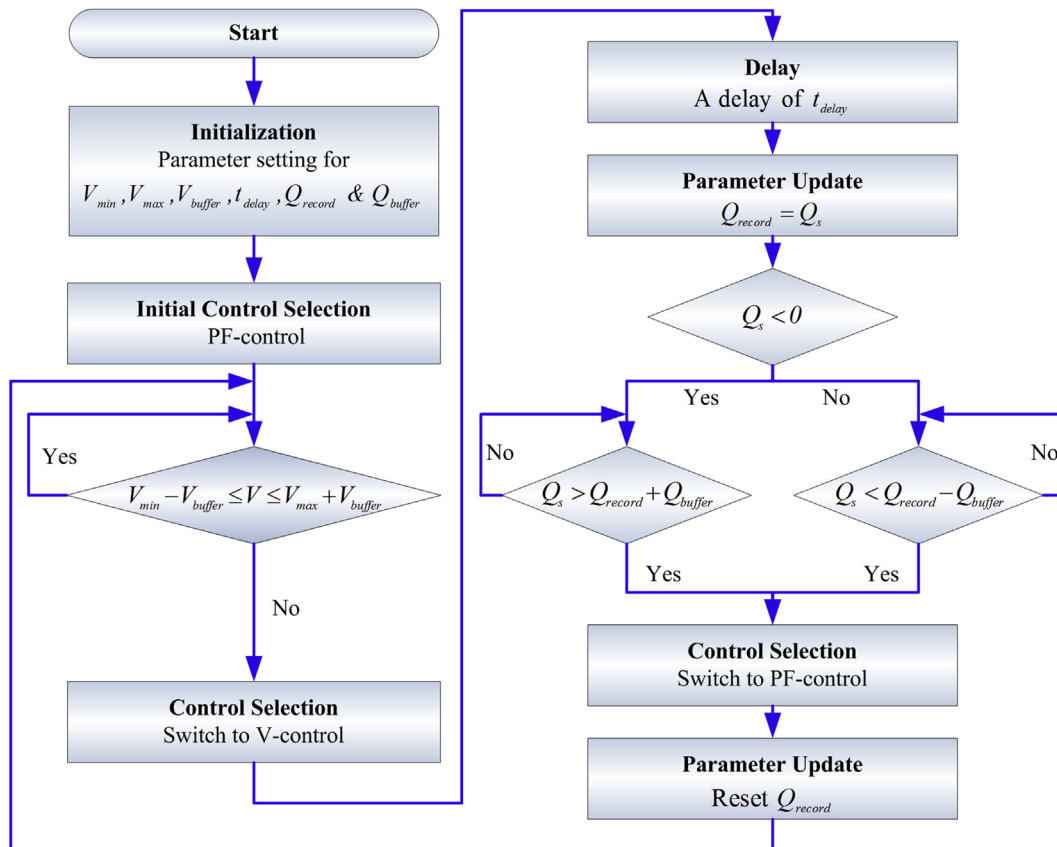


Fig. 13. Flowchart of the proposed multi-control selection algorithm.

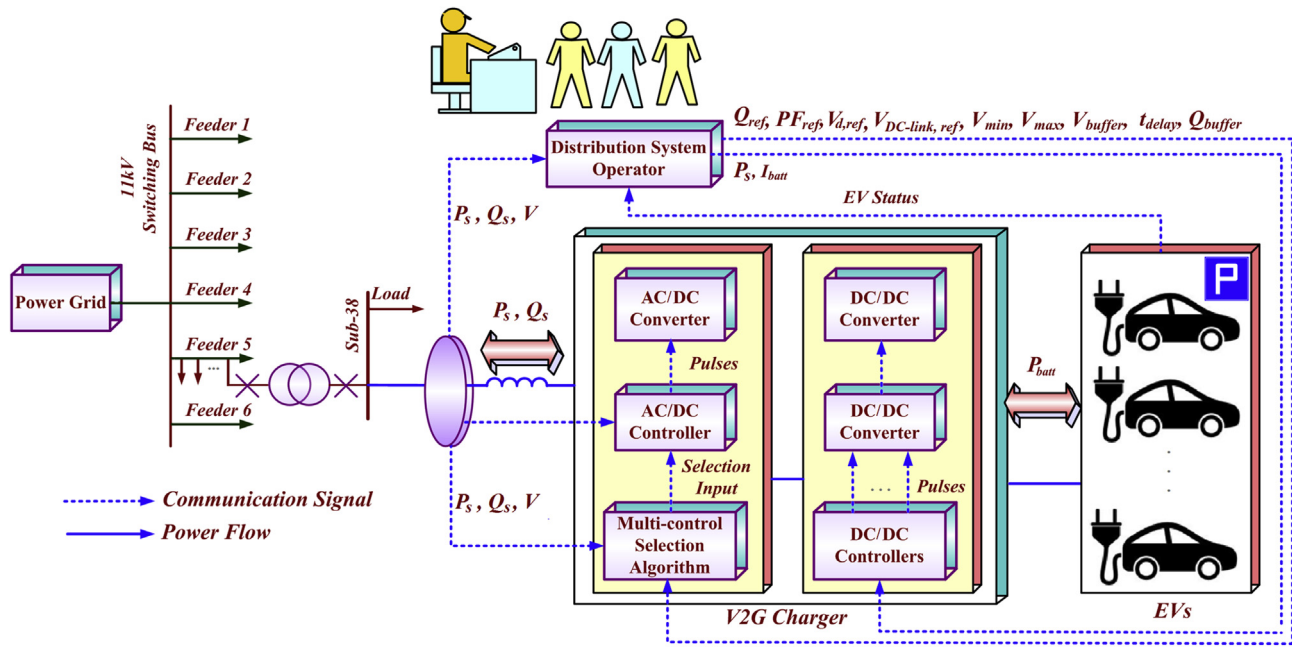


Fig. 14. Interaction between the proposed V2G charger, DSO and power grid for a practical V2G application.

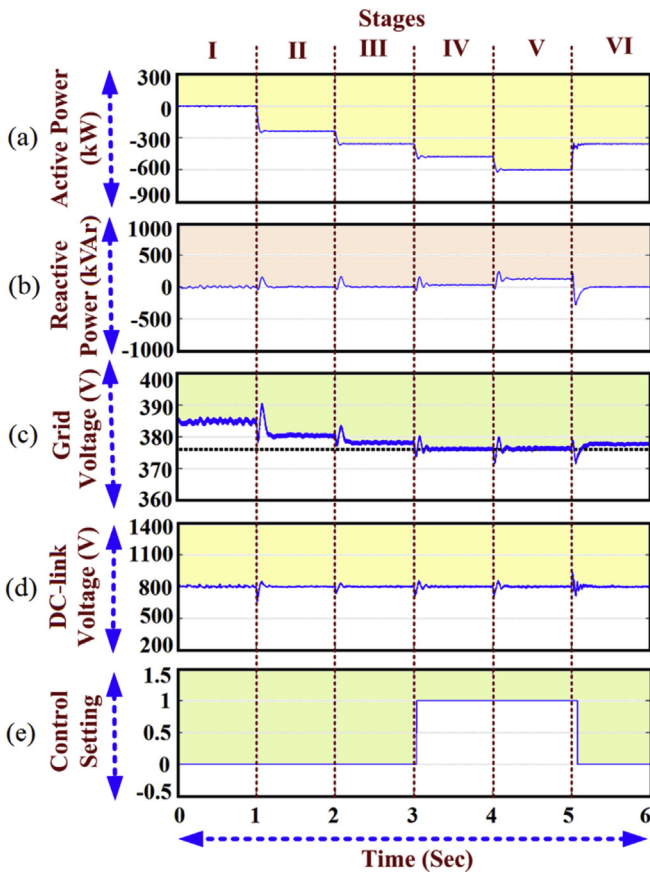


Fig. 15. Simulation results of the implementation of multi-control selection algorithm in V2G charger: (a) Active power, (b) Reactive power, (c) Grid voltage, (d) DC-link voltage and (e) Control setting.

In Stage-IV, a total of 12 EVs were connected to the V2G charger for EV charging. As shown in Fig 15(c), the grid voltage initially

dropped below the pre-set minimum grid voltage limit and eventually prompted the multi-control selection algorithm to switch to V-control (control setting = 1). The V2G charger successfully supplied an approximately 35 kVAR of reactive power to the grid for regulating the grid voltage to 376 V. Hence, the grid voltage violation due to fast charging of 12 EVs was solved. In Stage-V, the number of connected EVs to receive fast charging was further increased to 15 units, where V2G charger absorbed 600 kW of active power from the power grid to charge the vehicle batteries. In order to maintain the power grid voltage at 376 V, the supplied reactive power from the charger was increased to 125 kVAR. The V2G charger still operated in V-control (control setting = 1) since the condition to change to other controls was not fulfilled. In Stage-VI, the number of EVs to receive fast charging dropped to nine units. The active power drawn from the power grid to V2G charger apparently reduced. Consequently, the required reactive power for power grid voltage regulation also decreased. This situation had fulfilled the condition to switch the charger control back to unity PF-control (control setting = 0) as the grid voltage was significantly improved. Since the V-control was no longer required, the charger can be set to operate in an efficient control mode which was the unity PF-control. During this period, no reactive power flowed between the power grid and V2G charger. The grid voltage was 378 V which was higher than the minimum voltage limit. As shown in Fig 15(d), the DC-link voltage was maintained at 800 V throughout all stages of operation. The proposed multi-control selection algorithm successfully selected the practical charger control between PF-control and V-control to achieve efficient charger operations while complying with the power grid requirement.

### 6. Conclusion

This paper presented the design and development of a multi-control V2G charger with active and reactive power control for power grid supports. The proposed multi-control V2G charger utilized active power control to perform EV charging (C-control) and EV discharging (D-control); whilst utilized reactive power

control for power grid supports in terms of reactive power compensation (Q-control), power factor correction (PF-control), and grid voltage regulation (V-control). Extensive analyses were conducted under various scenarios and control modes to examine the performance of the charger controls. Simulation results showed that V2G operations at unity power factor (CPF1 and DPF1) marked the highest charger efficiency. Nonetheless, EV charging at unity power factor (CPF1) along with CQ3, CQ4, and CPF3 control modes introduced a significant voltage drop to the power grid, which violated the permissible grid voltage limit of  $-6\%$ . This problem can be overcome by implementing V-control in the V2G charger (CV1 and CV2) to provide an appropriate amount of reactive power from the charger to the power grid for accurate grid voltage regulation. On the other hand, EV discharging in all control modes did not cause a serious voltage rise problem.

This paper also proposed a multi-control selection algorithm to assist V2G charger in selecting the best charger control according to the power grid condition. Results showed that the proposed algorithm had effectively instructed V2G charger to operate in efficient control modes whenever the power grid voltage was within the permissible voltage limit of  $+10\%$  and  $-6\%$ . In the case of grid voltage violation, V-control was adopted by V2G charger to regulate the grid voltage to acceptable levels. This proposed multi-control V2G charger will be suitable to be implemented at any EV charging station, especially when involves large scale of charging event because it allows efficient EV charging as well as prevents voltage violation issue. Overall, the contributions of this paper were listed as follows:

- 1) A multi-control V2G charger with bi-directional active and reactive power for grid support was designed.
- 2) A multi-control selection algorithm for automatic switching between the multiple charger controls according to the power grid conditions was developed.
- 3) Thorough comparative analyses and technical assessments on the proposed charger controls under various scenarios were performed. These assessments were used to recommend the best practice of charger controls to meet specific objectives.

## Appendix A. Supplementary data

Supplementary data to this article can be found online at <https://doi.org/10.1016/j.energy.2019.01.053>.

## References

- [1] Markovska N, Duic N, Mathiesen BV, Guzovic Z, Piacentino A, Schlor H, Lund H. Addressing the main challenges of energy security in the twenty-first century – contributions of the conferences on sustainable development of energy, water and environment systems. *Energy Nov.* 2016;115:1504–12. <https://doi.org/10.1016/j.energy.2016.10.086>.
- [2] International Energy Agency, “Global EV Outlook 2016: Beyond one million electric cars,” Paris, France [Online]. Available: [https://www.iea.org/publications/free\\_publications/publication/Global\\_EV\\_Outlook\\_2016.pdf](https://www.iea.org/publications/free_publications/publication/Global_EV_Outlook_2016.pdf), Accessed on: May 3, 2017.
- [3] Nezamoddini N, Wang Y. Risk management and participation planning of electric vehicles in smart grids for demand response. *Energy Dec.* 2016;116: 836–50. <https://doi.org/10.1016/j.energy.2016.10.002>.
- [4] Falahati S, Taher SA, Shahidehpour M. A new smart charging method for EVs for frequency control of smart grid. *Int. J. Elec. Power Dec.* 2016;83:458–69. <https://doi.org/10.1016/j.ijepes.2016.04.039>.
- [5] Open Charge Map, “Navigate the world of electric vehicle charging,” [Online]. Available: <https://openchargemap.org/site>, Accessed on: Jul. 4, 2017.
- [6] Lund H, Kempton W. Integration of renewable energy into the transport and electricity sectors through V2G. *Energy Policy* Sept 2008;36:3578–87. <https://doi.org/10.1016/j.enpol.2008.06.007>.
- [7] Pfeifer A, Boskovic F, Dobravec V, Matak N, Krajacic G, Duic N, Puksec T. Building smart energy systems on Croatian islands by increasing integration of renewable energy sources and electric vehicles. In: *IEEE international conference on environment and electrical engineering and 2017 IEEE industrial and commercial power systems europe (EIEIC/I&CPS europe), milan, Italy, jun 6-9; 2017*.
- [8] Shojaabadi S, Abapour S, Abapour M, Nahavandi A. Simultaneous planning of plug-in hybrid electric vehicle charging stations and wind power generation in distribution networks considering uncertainties. *Renew Energy Dec.* 2016;99:237–52. <https://doi.org/10.1016/j.renene.2016.06.032>.
- [9] López MA, Torre SDL, Martín S, Aguado JA. Demand-side management in smart grid operation considering electric vehicles load shifting and vehicle-to-grid support. *Int. J. Elec. Power Jan.* 2015;64:689–98. <https://doi.org/10.1016/j.ijepes.2014.07.065>.
- [10] Paterakis NG, Erdinc O, Pappi IN, Bakirtzis AG, Catalão JPS. Coordinated operation of a neighborhood of smart households comprising electric vehicles, energy storage and distributed generation. *IEEE Trans. Smart Grid Nov.* 2016;7(6):2736–47. <https://doi.org/10.1109/TSG.2015.2512501>.
- [11] Ji Z, Huang X, Xu C, Sun H. Accelerated model predictive control for electric vehicle integrated microgrid energy management: a hybrid robust and stochastic approach. *Energies Nov.* 2016;9(11):973. <https://doi.org/10.3390/en9110973> (1–18).
- [12] Liu W, Hu W, Lund H, Chen Z. “Electric vehicles and large-scale integration of wind power – the case of inner Mongolia in China. *Appl Energy April* 2013;104:445–56. <https://doi.org/10.1016/j.apenergy.2012.11.003>.
- [13] You S, Hu J, Ziras C. An overview of modeling approaches applied to aggregation-based fleet management and integration of plug-in electric vehicles. *Energies Nov.* 2016;9(11):968. <https://doi.org/10.3390/en9110968> (1–18).
- [14] Kisacikoglu MC, Kesler M, Tolbert LM. Single-phase on-board bidirectional PEV charger for V2G reactive power operation. *IEEE Trans. Smart Grid Mar.* 2015;6(2):767–75. <https://doi.org/10.1109/TSG.2014.2360685>.
- [15] Metidji R, Metidji B, Mendil B. Design and implementation of a unity power factor fuzzy battery charger using an ultrasparse matrix rectifier. *IEEE Trans Power Electron May* 2013;28(5):2269–76. <https://doi.org/10.1109/TPEL.2012.2211107>.
- [16] Serra FM, Angelo CHD. IDA-PBC control of a single-phase battery charger for electric vehicles with unity power factor. In: *IEEE conference on control applications, buenos aires, Argentina, sep. 19-22; 2016*. p. 261–6.
- [17] Yong JY, Ramachandaramurthy VK, Tan KM, Mithulananthan N. Bi-directional electric vehicle fast charging station with novel reactive power compensation for voltage regulation. *Int. J. Elec. Power Jan.* 2015;64:300–10. <https://doi.org/10.1016/j.ijepes.2014.07.025>.
- [18] Tan KM, Ramachandaramurthy VK, Yong JY. Bidirectional battery charger for electric vehicle. In: *IEEE innovative smart grid technologies - asia, kuala lumpur, Malaysia, may 20-23; 2014*. p. 406–11.
- [19] Monteiro V, Pinto JG, Afonso JL. Operation modes for the electric vehicle in smart grids and smart homes: present and proposed modes. *IEEE Trans Veh Technol Mar.* 2016;65(3):1007–20. <https://doi.org/10.1109/TVT.2015.2481005>.
- [20] Vittorias I, Metzger M, Kunz D, Gerlich M, Bachmaier G. A bidirectional battery charger for electric vehicles with V2G and V2H capability and active and reactive power control. In: *IEEE transportation electrification conference and expo, dearborn, MI, USA, jun. 15-18; 2014*. p. 1–6.
- [21] Kim S, Kang FS. Multifunctional onboard battery charger for plug-in electric vehicles. *IEEE Trans Ind Electron Jun.* 2015;62(6):3460–72. <https://doi.org/10.1109/TIE.2014.2376878>.
- [22] Tanaka H, Ikeda F, Tanaka T, Yamada H, Okamoto M. Novel reactive power control strategy based on constant DC-capacitor voltage control for reducing the capacity of smart charger for electric vehicles on single-phase three-wire distribution feeders. *IEEE Trans. Emerg. Sel. Topics Power Electron. Jun.* 2016;4(2):481–8. <https://doi.org/10.1109/JESTPE.2015.2467379>.
- [23] Tan KM, Ramachandaramurthy VK, Yong JY. Three-phase bidirectional electric vehicle charger for vehicle to grid operation and grid voltage regulation. In: *IEEE transportation electrification conference and expo - asia-pacific, busan, South Korea, jun. 1-4; 2016*. p. 7–12.
- [24] Hung DQ, Dong ZY, Trinh H. Determining the size of PHEV charging stations powered by commercial grid-integrated PV systems considering reactive power support. *Appl Energy Dec.* 2016;183:160–9. <https://doi.org/10.1016/j.apenergy.2016.08.168>.
- [25] Yong JY, Fazeli SM, Ramachandaramurthy VK, Tan KM. Design and development of a three-phase off-board electric vehicle charger prototype for power grid voltage regulation. *Energy Aug.* 2017;133:128–41. <https://doi.org/10.1016/j.energy.2017.05.108>.
- [26] Yong JY, Ramachandaramurthy VK, Tan KM, Mithulananthan N. A review on the state-of-the-art technologies of electric vehicle, its impacts and prospects. *Renew Sustain Energy Rev Sept.* 2015;49:365–85. <https://doi.org/10.1016/j.rser.2015.04.130>.
- [27] Saadat H. *Power system analysis*. second ed. McGraw-Hill; 2004. p. 26–8.
- [28] J. Y. Yong, V. K. Ramachandaramurthy, K. M. Tan, and J. Selvaraj, “Experimental validation of a three-phase off-board electric vehicle charger with new power grid voltage control,” *IEEE Trans. Smart Grid*, to be published, 10.1109/TSG.2016.2617400.
- [29] Planning and design criteria (Part 5.4): steady-state supply voltage variation. *The Distribution Code for Peninsular Malaysia; 2016*.